Comprehensive Design and Optimization of an Onboard Resonant Self-Heater for EV Battery

Chong Zhu, *Member*, *IEEE*, Yue Cao, *Member*, *IEEE*, Hua Zhang, *Member*, *IEEE*, Fei Lu, *Member, IEEE*, and Xi Zhang, *Senior Member, IEEE*

***Abstract*—As the primary power sources of electric vehicles (EVs), lithium-ion batteries suffer from substantial capacity and power degradation at cold climates. An onboard battery preheater is essential for EVs to avoid degraded battery performance. This paper proposed a resonant battery self-heater for internally preheating the batteries without external power supplies, thereby providing great flexibility for EVs at different parking areas. To achieve the optimized performance, a detailed analytical model of the self-heater is derived, illustrating the effects of the switching frequency and resonant tank parameters. Considering the size, heating speed, and efficiency, the detailed design methodology of the proposed self-heater is presented by utilizing a nonlinear optimization method, in which the battery impedance variation is included. The downscaled experiments on 18650 cells validate that the optimally designed self-heater can warm up the batteries from -20 °C to 0 °C rapidly with the minimum energy consumption compared to previous heating schemes.**

***Index Terms*— Electric vehicles, lithium-ion battery, resonant power converter, cold start, resonant heating**

I. Introduction

Transportation industry is developing rapidly through the decades, leading to increased fossil energy consumption and emissions. To make transportation more sustainable, there has been tremendous progress moving toward electric vehicles (EVs) [1]. As the primary power source, traction batteries have a significant impact on the performance, safety, and economy of EVs. With the advantages of high power and energy density, long cycle life, low self-discharge rate, and negligible memory effect, lithium-ion (Li-ion) batteries are widely adopted as the energy storage component in EVs [2].

Li-ion batteries suffer from severe performance degradation under cold climates, especially at subzero Celsius. Due to reduced conductivity of the electrolyte, slow solid-state lithium diffusion, high polarization of graphite anode, and increased charge-transfer resistance, internal battery resistance increases considerably at conditions below -20 ºC, which leads to a drastic reduction in power sourcing/sinking capabilities [3-5]. With a cold start-up, EV driving ranges can be substantially shortened. More severely, the battery charging for EVs at extremely cold weather is also a potential risk, because the lithium plating at the anode face is likely to result in significant capacity loss or even internal short circuit [6-8].

To mitigate the range anxiety and safety concerns, it is essential to warm up the batteries for EVs before driving and charging in cold weather. Moreover, several fast charging techniques also demand rapid battery warm-up to reduce capacity fade during charging [9,10]. Various battery preheating methods have been carried out in literature. Among them, the internal heating methods utilize the batteries' impedance to generate electrochemical heat inside the cell, directly warming up the electrodes and electrolytes without the long heat transfer path from the battery surface to the interior [11-13]. Therefore, compared to external heating methods, the internal heating is a more promising approach, which can realize a faster speed, a higher efficiency, and a more uniform temperature distribution.

To evaluate the battery heating performance, a frequency-domain equivalent circuit model is developed to investigate the impacts of AC heating current frequency and amplitude [14]. Based on the equivalent circuit model, an optimized heating current frequency is determined to exploit the maximum heat generation rate under the cell polarization voltage constraint [15-17]. To avoid the capacity loss caused by the lithium plating during heating, an electrochemical model of Li-ion batteries is developed in [18] to regulate the heating current amplitude dynamically, so that the lithium-plating potential is not reached to avoid triggering any side reaction. In [19], an echelon heating strategy is proposed to increase the heating current amplitude adaptively with the rising temperature, so that the trade-off between the heat generation rate and the capacity fade rate is achieved during the internal heating.

Due to the slow diffusion characteristic, the low-frequency electrochemical impedance of Li-ion batteries at low temperatures is much higher than that at normal temperatures [20]. Therefore, the internal warm-up methods in [14-19] tend to utilize the AC current at the frequencies of 1-100 Hz to generate more electrochemical heat for shortening the heating time. Thus, an external power supply with large passive components, such as filtering inductors, should be provided for

Manuscript received May 15, 2020; revised Jul. 19, 2020 and Aug. 25, 2020; accepted Aug. 28, 2020.

C. Zhu and X. Zhang are with the School of Mechanical Engineering, Shanghai Jiao Tong University, Shanghai 200240, China. (E-mail: chong.zhu@sjtu.edu.cn; braver1980@sjtu.edu.cn).

Yue Cao is with the Energy Systems Group at Oregon State University, Corvallis, OR 97331, USA (E-mail: yue.cao@oregonstate.edu).

H. Zhang and F. Lu are with the Department of Electrical and Computer Engineering, Drexel University, PA 19104, USA (E-mail: hua.zhang@drexel.edu; fei.lu@drexel.edu)

This article has been accepted for publication in a future issue of this journal, but has not been fully edited. Content may change prior to final publication. Citation information: DOI 10.1109/TTE.2020.3025014, IEEE Transactions on Transportation Electrification

EVs to generate such AC current. This power supply endures additional cost and poor interoperability. To address this issue, there is a trend [21, 22] to utilize high-frequency onboard power converters to implement battery management. In [23-25], an interleaved half-bridge circuit topology is utilized to transfer energy between two series-connected battery strings, allowing AC heating current generated without external power supplies. This configuration is particularly suitable for an onboard battery self-heater.

Given limited space in EVs, the onboard power electronics enabled battery self-heaters prefer reduced passive components by operating at high frequencies up to 10-50 kHz. Hence, switching losses of the power semiconductor switches tend to dominant. The self-heaters proposed in [26-29] implement the series-resonant configurations to switching at the current peaks, realizing soft-switching capability. Moreover, large turn-on voltage or turn-off current, which may aggravate the breakdown of power switches, can be eliminated by soft switching.

Due to inherent merits of high efficiency, compact size, and reliability, the resonant battery self-heater (RBSH) is preferred for onboard implementations in EVs. However, RBSH parameter design challenges performance optimization, such as heating speed, efficiency, and reliability. These RBSH characteristics include peak heating current, soft-switching capability, and efficiency. Such parameters must be determined at the initial design stage because the battery management system (BMS) is hard to implement the signal sensing and closed-loop control in real-time due to the high operation frequencies. Some BMS monitored elements fail to incorporate with the RBSH control. One example is the electrochemical impedance of Li-ion batteries that varies with the temperature rise during internal heating, which has a noticeable impact on the RBSH performance. Such a multi-objective optimization problem is hard to acquire a global optimum without theoretical guidelines [30]. Therefore, a comprehensive design methodology and an optimization framework must guide for future work in RBSH. To the best of the authors' knowledge, few publications have addressed this need.

The main contribution of this paper is to develop a comprehensive RBSH design methodology, which simplifies the complicated multi-objective optimization into a single-objective problem. Thus, the RBSH performance in heating speed, efficiency, and reliability can be co-optimized. The rest of the paper is organized as follows. At first, the analytical model of the RBSH is investigated in detail. Based on the analytical expressions of the RBSH's time-domain waveforms, the effects of the switching frequency and resonant tank parameters are illustrated. By considering the component sizing, temperature-rise rate, soft-switching capability, and efficiency, the RBSH switching frequency, and resonant tank parameters are formulated as an optimization problem with constraints. Then, the Adaptive Genetic Algorithm is utilized to solve the nonlinear optimization problem for the optimum RBSH design, in which the temperature-dependent battery impedance is also taken into account. A design example of a downscaled RBSH for 18650 Li-ion cells is presented, and followed by the related experimental validation. The results show that the proposed optimal design can contribute to preheat the battery from -20 °C to 0 °C within 314s, and only consume 5.01% of the cell energy.

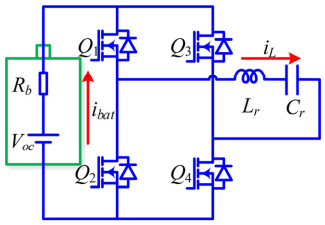

Fig. 1. Circuit topology of the proposed resonant battery self-heater.

II. Operation Principle of the RBSH

The main operating principle of the onboard RBSH is to utilize battery impedance to generate the electrochemical heat. Hence, it is essential to investigate the impedance model of Li-ion batteries for analyzing the warm-up performance of the RBSH. According to [31], the typical impedance of Li-ion batteries appears close to a pure resistor at high frequencies (1 to 50 kHz). Since the RBSH operates within 1-50 kHz, it is reasonable to simplify the Li-ion battery model to a state-of-charge (SOC) dependent voltage source V_b in series with an internal resistor R_b.

The proposed onboard RBSH is based on an H-bridge topology, as shown in Fig. 1. The terminals of the battery pack connect to the DC nodes of the converter, and a series-connected resonant tank (L_r and C_r) connects to the phase legs. A group of complementary PWM signals, at duty ratios of 0.5, are provided for Q_1/Q_4 and Q_2/Q_3. This topology allows the energy to be transferred from the battery pack to the resonant tank, and *vice versa*. Therefore, the alternate charge/discharge current can be generated for heating cells without external power supplies.

There are two operation states of the RBSH. During state I, power switches Q_1 and Q_4 are turned on, while Q_2 and Q_3 are turned off. The battery module's cathode and anode are in forwarding connection with the resonant tank L_r and C_r. Thus, the circuit equation can be expressed as:

$$\begin{cases} V_{oc} = R_b i_{bat} + R_{loss} i_L + L_r \dfrac{di_L}{dt} + v_c \\ i_L = C_r \dfrac{dv_c}{dt} \\ i_{bat} = i_L \end{cases} \tag{1}$$

where R_{loss}=$2R_{ds(on)}$+R_L+R_c is used to represent the conduction loss of the switches and the power loss of the resonant tank. During state II, Q_2 and Q_3 are turned on, while Q_1 and Q_4 are turned off. Hence, the battery module's cathode and anode are connected with the resonant tank L_r and C_r reversely. The circuit equation can be expressed as:

$$\begin{cases} V_{oc} = R_b i_{bat} - R_{loss} i_L - L_r \dfrac{di_L}{dt} - v_c \\ i_L = C_r \dfrac{dv_c}{dt} \\ i_{bat} = -i_L \end{cases} \tag{2}$$

This article has been accepted for publication in a future issue of this journal, but has not been fully edited. Content may change prior to final publication. Citation information: DOI 10.1109/TTE.2020.3025014, IEEE Transactions on Transportation Electrification

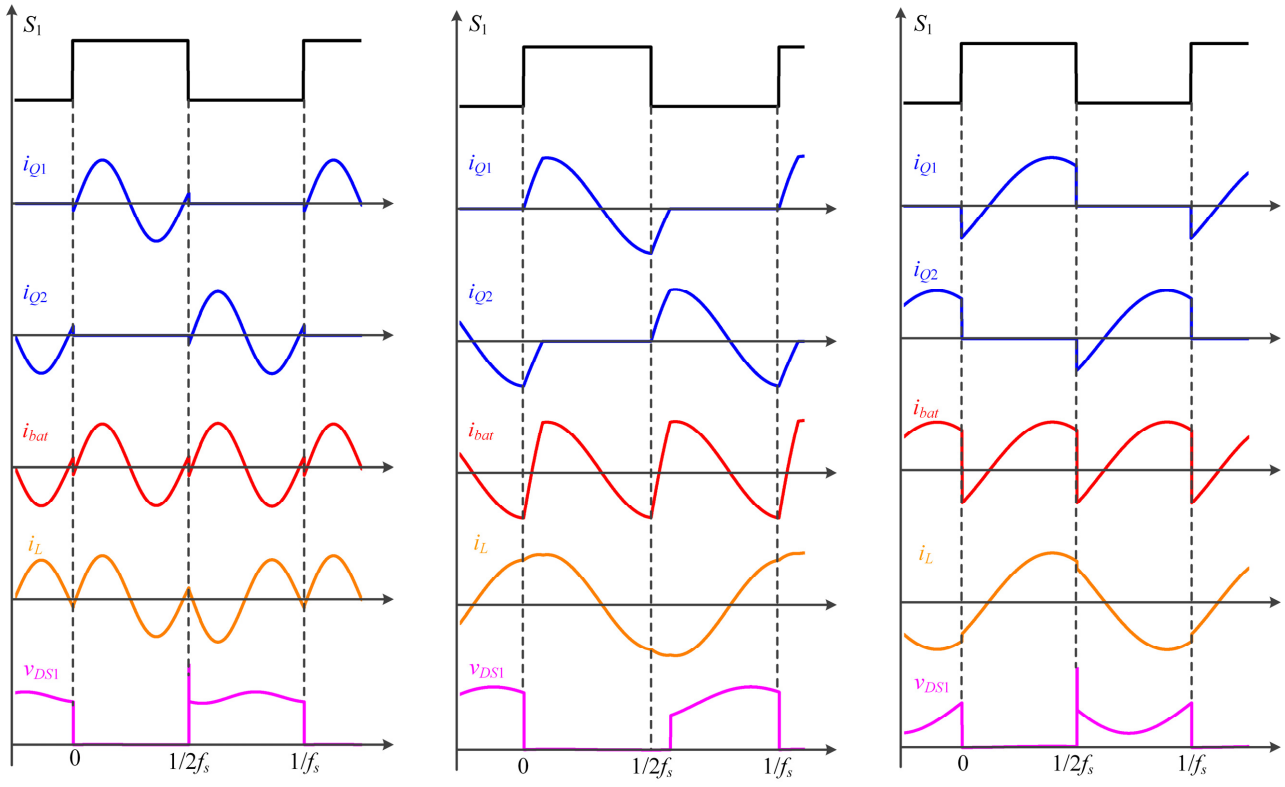

Fig. 2. Waveforms of the proposed resonant battery self-heater: (a) $f_s>f_r$; (b) $f_r/2<f_s<f_r$; (c) $f_s<f_r/2$.

Depending on switching frequency f_s, the operating conditions of the RBSH are varied. In general, resonant converters operate with a switching frequency slightly higher than the resonant frequency ($f_r=1/2\pi\sqrt{L_rC_r}$) of the series LC branch, because the zero-voltage-switching (ZVS) characteristic can be achieved to eliminate turn-on losses and improve the reliability. However, for RBSHs, there is no active power transferred from the resonant tank to an actual load, so that the power factor of the converter's AC side is nearly zero. This undesirable feature leads to power switches cut-off at the current peaks, degrading their reliability due to undesirable cut-off voltage spikes, as shown in Fig. 2(a). Furthermore, the low equivalent impedance of the resonant tank leads to almost short-circuit of the cells, so that this operation mode ($f_s>f_r$) cannot be applied for the RBSHs.

When f_s is slightly lower than the resonant frequency f_r, the turn-off current for power switches is always negative, as shown in Fig. 2(b). Thus, the ZVS characteristic cannot be obtained by the RBSHs, which is not desirable for high-frequency applications.

In order to achieve the desired ZVS capability, f_s must be further reduced to lower than $f_r/2$. In such cases, the phase angle of the output current i_L lags that of the output voltage, so that the turn-off current can be regulated to fulfill the ZVS requirement, as shown in Fig. 2(c). Meanwhile, at this mode, the equivalent impedance of the resonant tank varies with f_s, which can be carefully designed to regulate the heating current i_{bat}. As a result, this operation mode ($f_s<f_r/2$) is preferred for the RBSH applications. The detailed analysis and design principle will be discussed in the next section.

III. Design Consideration of the RBSH

A. Modeling of the RBSH

Given that the RBSH operates at the switching frequency f_s lower than $f_r/2$, as shown in Fig. 2(c). Thus, the analytical solution of the differential equations (1) and (2) can be expressed by

$$\begin{cases} v_c = e^{-\tau t}\left(\beta_1\cos\omega_h t+\beta_2\sin\omega_h t\right)+V_{oc} \\ i_L = C_r\dfrac{dv_c}{dt} \\ \quad = C_r e^{-\tau t}\left[\left(\tau\beta_1+\omega_h\beta_2\right)\cos\omega_h t+\left(\tau\beta_2-\omega_h\beta_2\right)\sin\omega_h t\right] \end{cases} \tag{3}$$

where

$$\begin{cases} \tau = \dfrac{R_b+R_{loss}}{2L}=\dfrac{\omega_r\left(R_b+R_{loss}\right)}{2Z_r} \\ \omega_h = \sqrt{\dfrac{1}{L_rC_r}-\dfrac{\left(R_b+R_{loss}\right)^2}{4L_r^2}}=\omega_r\sqrt{1-\dfrac{\left(R_b+R_{loss}\right)^2}{4Z_r^2}} \end{cases} \tag{4}$$

In (4), $\omega_r=\sqrt{1/L_rC_r}$ denotes the resonant frequency of the series resonant tank, and $Z_r=\sqrt{L_r/C_r}$ denotes the characteristic impedance of the resonant tank. By considering the energy conservation principle of the resonant tank, the initial condition of (1) and (2) can be represented by $i_L(0)=-i_L(1/2f_s)$ and $v_c(0)=-v_c(1/2f_s)$. Thus, the analytical solution of the

This article has been accepted for publication in a future issue of this journal, but has not been fully edited. Content may change prior to final publication. Citation information: DOI 10.1109/TTE.2020.3025014, IEEE Transactions on Transportation Electrification

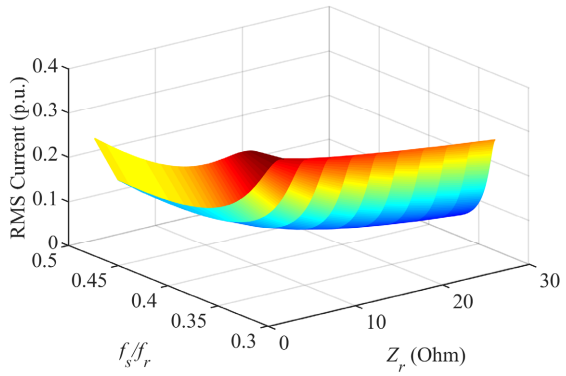

Fig. 3. RMS heating current at different switching frequencies and characteristic impedances.

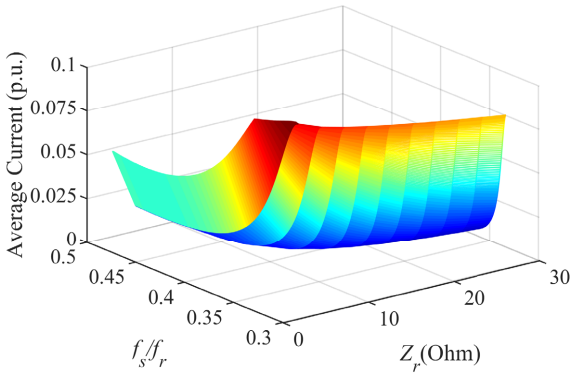

Fig. 4. Average heating current at different switching frequencies and characteristic impedances.

heating current at state I ($0<t<1/2f_s$) can be derived as

$$i_{bat}(t)=i_L(t)=\frac{\omega_r V_{oc} e^{-\tau t}}{\omega_h Z_r\left(1+e^{-\frac{\tau}{f_s}}+2e^{-\frac{\tau}{2f_s}}\cos\frac{\omega_h}{2f_s}\right)}\cdot \left[\sin\omega_h t+e^{-\frac{\tau}{2f_s}}\sin\omega_h\left(t-\frac{1}{2f_s}\right)\right] \tag{5}$$

As the heating current at state II ($1/2f_s<t<1/f_s$) is symmetrical with that at state I, we can just focus on the analytical solution in the first state without loss of generality.

B. Parametrized performance of the RBSH

Since the RBSH utilizes the AC current to generate the electrochemical heat, the heating power is directly determined by the root-mean-square (RMS) value of the heating current. According to (5), the RMS heating current can be calculated by

$$I_{RMS}=\sqrt{2f_s\int_0^{1/2f_s} i_{bat}^2(t)dt}=\frac{V_{oc}}{Z_r}\sqrt{\frac{f_s}{2\tau}\cdot\frac{\omega_h\left(1-e^{-\frac{\tau}{f_s}}\right)-2\tau e^{-\frac{\tau}{2f_s}}\sin\frac{\omega_h}{2f_s}}{1+e^{-\frac{\tau}{f_s}}+2e^{-\frac{\tau}{2f_s}}\cos\frac{\omega_h}{2f_s}}} \tag{6}$$

According to (6), the influence of f_s and Z_r on the RMS heating current can be depicted in Fig. 3. The calculated RMS heating current is expressed by the per-unit (p.u.) value, where the open-circuit voltage V_{oc} and battery internal resistance R_b are taken as 1 V and 1 Ω, respectively. The losses of the passive components L_r and C_r are calculated with the fixed quality factor Q_L and Q_c, which are represented by $R_L=\omega_r L/Q_L$ and $R_c=1/Q_c\omega_r C$. As shown in the figure, I_{RMS} is monotone decreased with the increasing Z_r due to the voltage-source characteristic of the proposed RHSB. In contrast, the influence of the switching frequency f_s is not monotonic at the range between $f_r/3$ and $f_r/2$. When f_s is close to $f_r/2$, I_{RMS} increases with the rising switching frequency due to the falling equivalent capacitive impedance of the resonant tank. On the other hand, when f_s approaches near $f_r/3$, its effect on I_{RMS} is inversed. This high heating current is induced by the 3rd-order harmonic of the RBSH output voltage, whose equivalent load impedance around $f_r/3$ is almost zero. Due to the sharp impedance characteristic around the resonant operation point, I_{RMS} is quite sensitive around $f_s=f_r/3$. Thus, it is essential to pay extra attention to choose a proper f_s for the required RMS heating current.

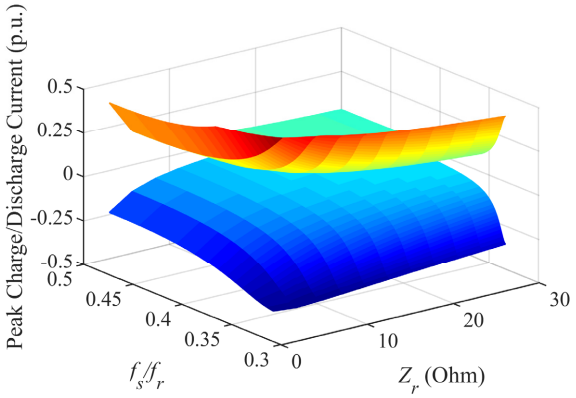

Fig. 5. Peak charge/discharge current at different switching frequencies and characteristic impedances.

To evaluate the total output power of Li-ion batteries during self-heating, the average heating current should be derived, which is expressed by

$$I_{AVG}=2f_s\int_0^{1/2f_s} i_{bat}(t)dt=\frac{2V_{oc}f_s}{\omega_r\omega_h Z_r}\cdot\frac{\omega_h\left(1-e^{-\frac{\tau}{f_s}}\right)-2\tau e^{-\frac{\tau}{2f_s}}\sin\frac{\omega_h}{2f_s}}{1+e^{-\frac{\tau}{f_s}}+2e^{-\frac{\tau}{2f_s}}\cos\frac{\omega_h}{2f_s}} \tag{7}$$

Based on (7), the influence of f_s and Z_r on the average heating current I_{AVG} is depicted in Fig. 4. The effect of f_s on I_{AVG} is similar to that on I_{RMS}: I_{AVG} decreases with the increasing f_s near $f_r/3$, while it increases with the increasing f_s near $f_r/2$. With respect to Z_r, its effect is also not monotonic, because the losses of the resonant tank L and C increase with the growing Z_r considering the quality factors Q_L and Q_c. Therefore, I_{RMS} increase only a little with the growing I_{AVG} at a high Z_r range ($Z_r>15$), because substantial battery energy is consumed on the resonant tank. In other words, the efficiency of the RBSH is relatively low when Z_r is too high. In the design, high Z_r values should be eliminated to reduce self-heating energy consumption.

Meanwhile, the peak charge and discharge currents of the Li-ion battery during heating can also be calculated by finding the

This article has been accepted for publication in a future issue of this journal, but has not been fully edited. Content may change prior to final publication. Citation information: DOI 10.1109/TTE.2020.3025014, IEEE Transactions on Transportation Electrification

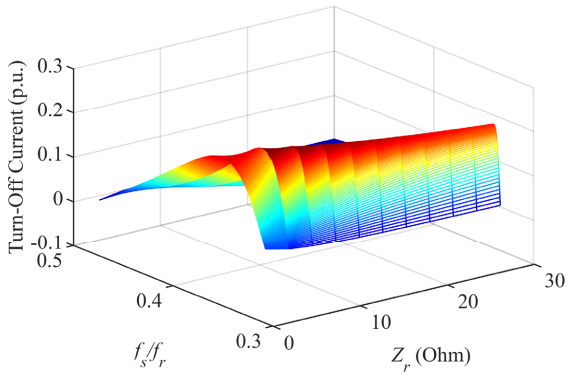

Fig. 6. Turn-off current at different switching frequencies and characteristic impedances.

derivatives of (5):

$$\begin{cases} I_{ch\_max} = i_{bat}(t_{ch}), & \left.\dfrac{di_{bat}(t)}{dt}\right|_{t=t_{ch}} = 0 \text{ and } \dfrac{d^2 i_{bat}(t)}{dt^2} > 0 \\ I_{dis\_max} = i_{bat}(t_{dis}), & \left.\dfrac{di_{bat}(t)}{dt}\right|_{t=t_{dis}} = 0 \text{ and } \dfrac{d^2 i_{bat}(t)}{dt^2} < 0 \end{cases} \tag{8}$$

By neglecting the attenuation item $e^{-\tau t}$ in (5), the peak charge and discharge currents can be approximately expressed by

$$\begin{cases} I_{ch\_max} = \dfrac{-\omega_r V_{oc} e^{-\frac{\tau(3\pi+2\varphi)}{2\omega_h}}}{\omega_h Z_r \sqrt{1+e^{-\frac{\tau}{f_s}}+2e^{-\frac{\tau}{2f_s}}\cos\dfrac{\omega_h}{2f_s}}} \\ I_{dis\_max} = \dfrac{\omega_r V_{oc} e^{-\frac{\tau(\pi+2\varphi)}{2\omega_h}}}{\omega_h Z_r \sqrt{1+e^{-\frac{\tau}{f_s}}+2e^{-\frac{\tau}{2f_s}}\cos\dfrac{\omega_h}{2f_s}}} \end{cases} \tag{9}$$

where

$$\varphi = \arctan\frac{e^{-\frac{\tau}{2f_s}}\sin\dfrac{\omega_h}{2f_s}}{1+e^{-\frac{\tau}{2f_s}}\cos\dfrac{\omega_h}{2f_s}} \tag{10}$$

In Fig. 5, the effects of f_s and Z_r on the peak charge and discharge currents are presented. The influence of f_s exhibits a similar tendency with that on I_{RMS}. In addition, the peak charge and discharge currents are decreased by the enlarged Z_r. The peak charge and discharge currents are the main limitations of the Li-ion batteries at cold climates, which will be fully considered as a constraint for the RBSH design.

Concerning the soft-switching capability, it is essential to study the turn-off current of the power switches during heating. According to the RBSH circuit topology, the turn-off current of switch Q_1 is equivalent to the heating current i_{bat} at t=1/2f_s. Thus, the current can be calculated by

$$i_{off} = i_{bat}\left(\frac{1}{2f_s}\right) = \frac{\omega_r V_{oc}}{\omega_h Z_r\left(1+e^{-\frac{\tau}{f_s}}+2e^{-\frac{\tau}{2f_s}}\cos\dfrac{\omega_h}{2f_s}\right)}\sin\frac{\omega_h}{2f_s} \tag{11}$$

To guarantee the ZVS characteristic, i_{off} must be positive to discharge the output capacitance of the power switch. As seen in Fig. 6, f_s must be drifted away from f_r/2 to avoid the negative turn-off current. The reason is that the actual heating current frequency ω_h is slightly lower than the resonant frequency ω_r due to the impact of the series resistances, leading to a negative value of i_L at the turn-off internal. Compared to f_s, Z_r has a minor impact on the turn-off current, which can be neglected in the following analysis.

C. Design consideration of the RBSH

Since the closed-loop control of the RBSH is difficult to achieve with a low-sample-rate BMS, the RBSH usually operates at a fixed switching frequency to warm up Li-ion batteries. Thus, the design parameters of the RBSH, namely, the resonant frequency f_r, switching frequency f_s, and characteristic impedance Z_r, have a decisive impact on the battery heating performance. The comprehensive design considerations for the RBSH is presented to obtain the optimized performance, such as its size, heating speed, efficiency, and soft-switching capability

1) Battery capacity losses

The peak charge and discharge currents, which are the primary concern for the durability of Li-ion batteries, should be constrained during self-heating to prevent battery capacity losses at low temperatures. I_{ch} and I_{dis} at low temperatures should follow battery manufacturers' instructions to avoid overpotential of lithium-plating. According to (9), f_s and Z_r should be designed to maintain I_{ch} and I_{dis} within the safety thresholds.

2) Heating speed

In general, the heating speed is the most concerning performance for EV battery warm-up. The heating speed of the RBSH is contributed by the RMS heating current, whose analytical model is represented by (5). Generally, a high RMS heating current is preferred for rapid battery heating speed. The design goal is to achieve the maximum possible I_{RMS} by tuning f_s and Z_r. However, the upper limit of I_{RMS} is saturated by the peak charge/discharge currents I_{ch} and I_{dis} to avoid undesirable cycling capacity fade. Based on the analytical model of the RBSH in (8), the RMS heating current increases with the rising switching frequency f_s near f_r/2. Alternatively, tuning f_s approaching to f_r/3 can also increase the RMS heating current. Therefore, it is desirable to tune f_s as close to f_r/2 or f_r/3 as possible and incorporate a proper Z_r to speed up the warm-up process. However, the effect of temperature-dependent battery impedance should also be considered when choosing the f_s range, which is discussed later.

3) Self-heating efficiency

The battery self-heating efficiency denotes the percentage of energy drawn from batteries that are utilized to generate the electrochemical heat. The efficiency of the RBSH can be calculated by

$$\eta = \frac{I_{RMS}^2 R_b}{V_{oc} I_{AVG}} = \frac{R_b}{R_b + R_{ds(on)} + Z_r\left(\dfrac{1}{Q_L}+\dfrac{1}{Q_c}\right)} \tag{12}$$

Assuming Q_L and Q_c are constant with a specific f_r, the

This article has been accepted for publication in a future issue of this journal, but has not been fully edited. Content may change prior to final publication. Citation information: DOI 10.1109/TTE.2020.3025014, IEEE Transactions on Transportation Electrification

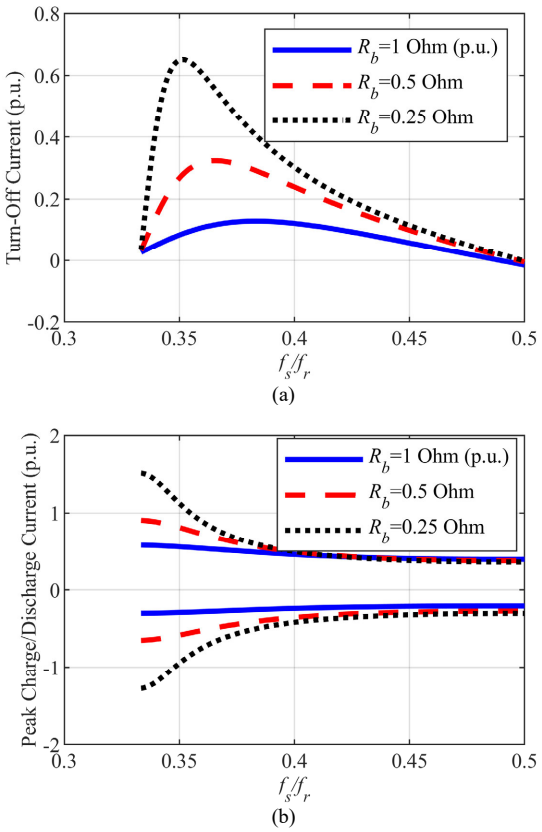

Fig. 7. Effect of battery impedance on the RBSH performance: (a) peak charge/discharge currents; (b) turn-off current.

efficiency can be improved by choosing a smaller characteristic impedance, because the losses of the resonant components are reduced. Since ω_h>0 must be guaranteed, the lower limit of Z_r can be derived from (4):

$$Z_{r\_min} = \frac{R_b + R_{ds(on)}}{2 - \frac{1}{Q_L} - \frac{1}{Q_c}} \tag{13}$$

However, Z_{r_min} cannot be always achievable in a practical RBSH to maximize the efficiency, because the design of Z_r should also be constrained by peak charge/discharge current limits, as explained in Section III-*C*. The actually implemented Z_r must be carefully calculated to prevent battery capacity loss.

4) ZVS capability

The soft-switching capability should also be considered to improve system efficiency as well as the reliability of the RBSH at high-frequency operation. The turn-off current of the RBSH must be sufficiently large to fully discharge the junction capacitance C_{oss} of the power switches within a deadtime t_d, so that the drain-to-source voltages (V_{DS}) of off-state switches drop to zero before the turn-on gate signals. In such a way, the ZVS operation of the power switches during turn-on transitions can be achieved to eliminate turn-on losses. From [32], it is clear that the discharge energy of C_{oss} is provided entirely by the inductor current. Considering that i_L must keep positive within t_d to avoid recharging C_{oss}, the minimum allowable turn-off current must be large enough when assuming i_L linearly decreases within t_d:

$$\int_0^{t_d} i_L dt \geq \frac{i_{off\_min} t_d}{2} \geq 2Q_{oss} = 2C_{oss} V_{oc} \tag{14}$$

Hence, the minimum allowable turn-off current can be calculated by:

$$i_{off\_min} = \frac{4C_{oss} V_{oc}}{t_d} \tag{15}$$

Based on (11), f_s should be carefully tuned to obtain a proper i_{off} for the ZVS characteristic.

5) Self-heater physical sizing

Due to limited space in EVs, the compactness of the RBSH is essential for onboard installation. Since the sizes of resonant components are dominant in the RBSH, f_r can be determined according to the specific space limitation in EVs. However, f_r cannot be too high due to considerable power losses of resonant components at high frequencies. In addition, at ultra high frequencies (>100 kHz), the impedance of lithium-ion batteries appears inductive. The inductive impedance characteristic leads to a high equivalent impedance of lithium-ion batteries at ultra high frequencies. With the same heating current magnitude, the inductive impedance is more likely to trigger the lithium-plating potential when the heating-current frequency is too high. To avoid capacity fade, the heating current madgitude should be tuned lower, thereby degrading the heating power. Hence, the upper limit of the heating frequency is clamped to 40-50 kHz to gain a higher battery heating speed without SOH degradation.

D. Effect of Battery Impedance Variation During Self-Heating

The impedance of Li-ion batteries is temperature-dependent, which is gradually reduced with the rising temperature during self-heating. According to (9)-(11), the reduced battery impedance is likely to cause over-current if f_s is not properly selected. Meanwhile, the turn-off current is affected by the diminished battery impedance as well. As shown in Fig. 7(a), the peak charge/discharge currents are strongly coupled with the temperature-dependent R_b near f_s=f_r/3, because the equivalent load impedance around f_s=f_r/3 is primarily determined by the battery impedance considering the 3rd-order voltage harmonics. In comparison, I_{ch} and I_{dis} are less sensitive to the temperature rise when f_s is close to f_r/2, where the equivalent load impedance is almost clamped to Z_r. Consequently, f_s should be carefully designed around f_r/2, i.e., 0.40f_r<f_s<0.5f_r, to avoid the lithium-plating caused by the over-current. Similar to the turn-off current, the temperature rise likely improves the ZVS condition, as shown in Fig. 7(b). Therefore, the soft-switching capability at the lowest temperature should be examined first in the design.

IV. Design Methodology of the RBSH

In Section III, the parameters of the RBSH are analyzed, whose impacts on the overall performance of the self-heater are presented in detail. The resonant frequency f_r, switching frequency f_s, and characteristic impedance Z_r have coupled effects on the heating speed, efficiency, and soft-switching capability. The tuning of f_r, f_s, and Z_r seems not straightforward

This article has been accepted for publication in a future issue of this journal, but has not been fully edited. Content may change prior to final publication. Citation information: DOI 10.1109/TTE.2020.3025014, IEEE Transactions on Transportation Electrification

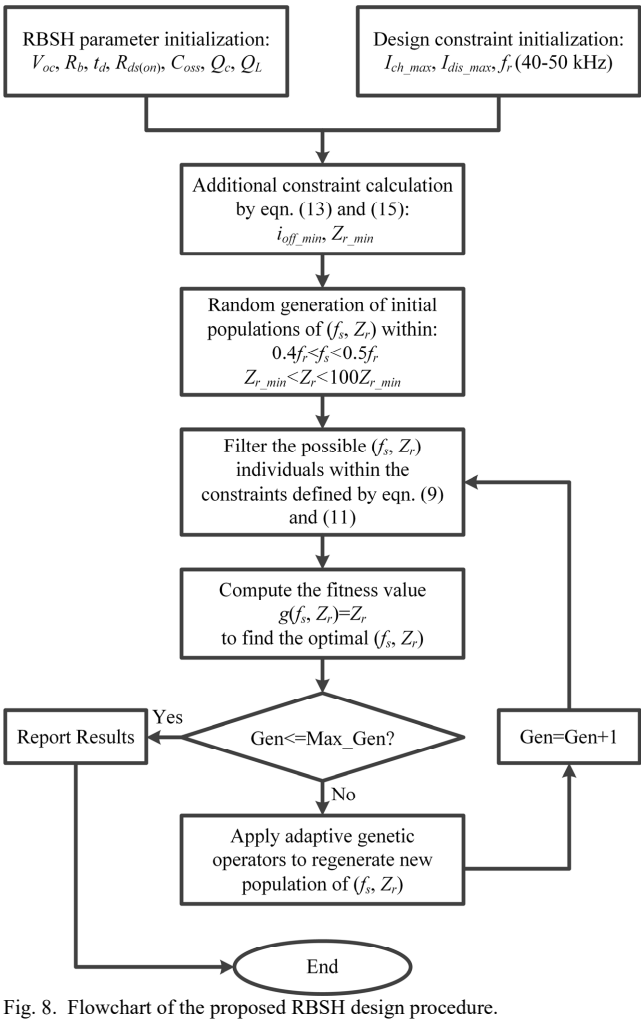

Fig. 8. Flowchart of the proposed RBSH design procedure.

TABLE I.
DESIGN CONSTRAINTS AND THE OPTIMIZED PARAMETERS OF THE RBSH

Design Constraints		Optimized RBSH Parameters	
Maximum charge/discharge current I_{ch_max}/I_{dis_max}	-9A/9A	Characteristic impedance Z_r	1.5 Ω
Minimum turn-off current i_{off_min}	0.0912 A	Resonant tank L_r/C_r	6.0μH/2.66μF
Minimum characteristic impedance Z_{r_min}	0.218 Ω	Switching frequency f_s	16.8 kHz

for the self-heater. Hence, an intuitive approach is presented here for the RBSH parameter design.

The first step is to choose f_r according to the specific space limitation in EVs. As described before, f_r should be within the range between 40 kHz and 50 kHz. A relatively high f_r can be selected at first to meet the sizing requirement, providing a base value for the other parameter design. A practical

Then, f_s and Z_r can be tuned based on the analytical model shown in (9)-(12). The major constraint of the RBSH is the peak charge/discharge current for the battery health guarantee. Since the effects of f_s and Z_r on I_{RMS} show almost the same tendency with that on I_{ch} and I_{dis}, the intuitive design approach is to tune f_s and Z_r for achieving the maximum possible I_{ch} and I_{dis}, as well

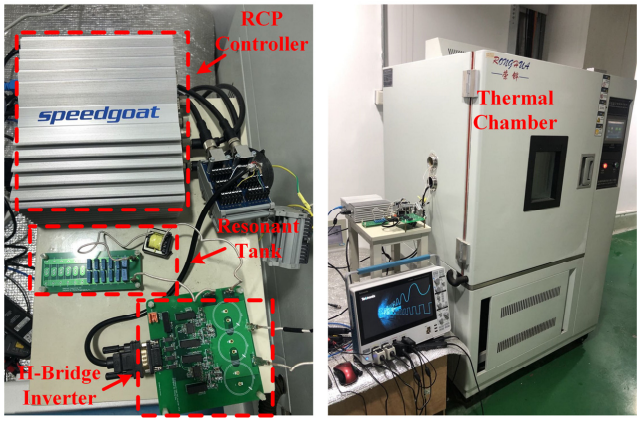

Fig. 9. Experimental setup of the proposed RBSH.

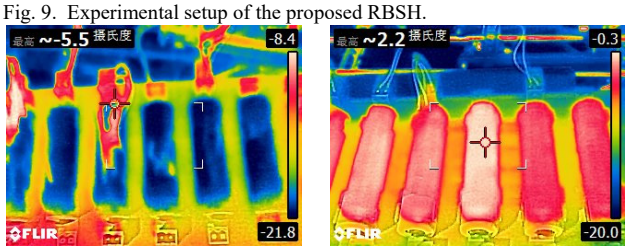

(a) (b)

Fig. 10. Thermal images of the tested battery cells: (a) before self-heating; (b) after self-heating.

as I_{RMS}. In this way, the maximum heating speed is achieved for warming up Li-ion batteries.

There are many possible combinations of f_s and Z_r that can achieve the maximum available I_{RMS}, so that additional constraints are required to optimize the parameters. According to (12), lower Z_r can contribute to improving the system efficiency. Therefore, the parameter design can be formulated to an optimization problem, in which the minimum Z_r is required with the given conditions, such as the maximum charge/discharge current and switching frequency range. Additionally, the ZVS capability described by (15) is also considered as a constraint.

The optimization problem can be described by

$$\begin{aligned} &min\ \ g(f_s, Z_r) = Z_r \\ &s.t.\ I_{ch\_max}(f_s, Z_r) \ge I^*_{ch\_max} \\ &\quad I_{dis\_max}(f_s, Z_r) \le I^*_{ch\_max} \\ &\quad i_{off}(f_s, Z_r) \ge i_{off\_min} \\ &\quad 0.4f_r \le f_s \le 0.5f_r \\ &\quad Z_r \ge Z_{r\_min} \end{aligned} \tag{16}$$

It should be noted that the constraint of f_s in (16) is to alleviate the influence of the impedance variation during the temperature rise. Also, i_{off} is calculated with the battery impedance at the low ambient temperature, which is the worst case for the ZVS condition. Combining (9)-(14), the optimized f_s and Z_r can be obtained by solving the optimization problem described by (15). The framework of the proposed design methodology is shown in Fig. 8.

Since most of the analytical equations in (9)-(14) are nonlinear, a nonlinear programming algorithm is applied here. Since the Adaptive Genetic Algorithm (AGA) is particularly suitable to search the global optimum of a constrained optimization, it is utilized to find the optimal f_s and Z_r in this

This article has been accepted for publication in a future issue of this journal, but has not been fully edited. Content may change prior to final publication. Citation information: DOI 10.1109/TTE.2020.3025014, IEEE Transactions on Transportation Electrification

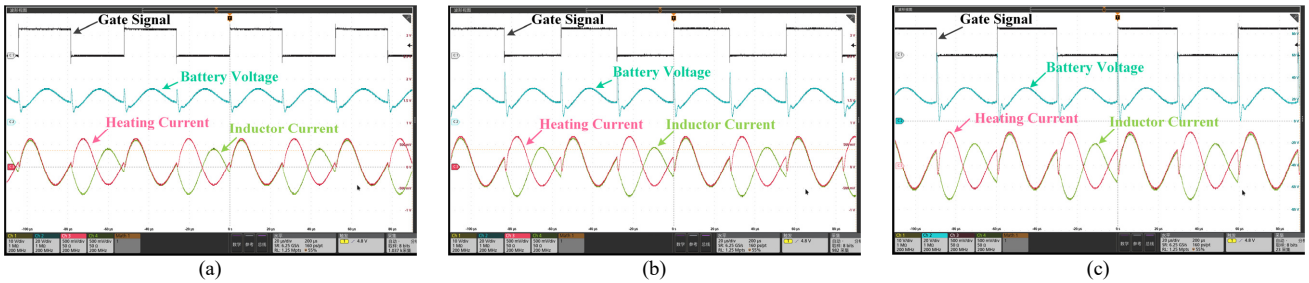

(a) (b) (c)

Fig. 11. Experimental waveforms of the RBSH with Z_r=2.4 Ω: (a) f_s=19.8 kHz; (b) f_s=18.0 kHz, (c) f_s=16.8 kHz.

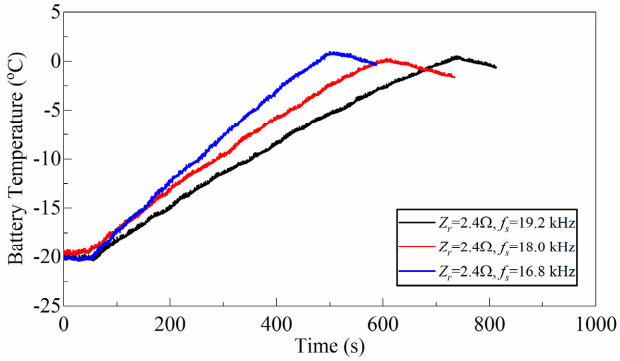

Fig. 12. Battery temperature during self-heating with Z_r=2.4 Ω.

paper [33]. The initial populations (f_s, Z_r) are converted into binary codes and located in the range of $0.4f_r<f_s<0.5f_r$ and $Z_{r\_min}<Z_r<100Z_{r\_min}$. The individuals out of the constrained zone defined by Eqn. (9)-(15) are filtered out, while the fitness value $g(f_s, Z_r)=Z_r$ is then evaluated with the remaining individuals in the population. Following this, the individuals with better adaptivity (lower fitness value) are reproduced for the next generation. Meanwhile, the cross and variation operations are also conducted by applying bit manipulations on the binary codes of individuals to improve the whole population's adaptivity. After several generations, the population (f_s, Z_r) can converge to the minimum possible Z_r with the nonlinear constraints. The iterative global optimal search can be terminated, and the optimal f_s and Z_r are determined to improve the overall RBSH performance.

V. Experimental Validation

To validate the proposed optimized design, the downscaled test bench of the RBSH is built, as shown in Fig. 9. The Transphorm GaN FETs TP65H035WS are used as power switches, whose R_{ds_on} and C_{oss} are 35 mΩ and 190 pF, respectively. The deadtime of the RBSH is set to 200 ns. For simplicity and generality, six LG 3Ah 18650 $LiNiMnCoO_2$ cells are connected in series to emulate an EV's battery pack, whose R_b at -20 ° C is 65 mΩ. The battery temperature is measured via the negative-temperature-coefficient (NTC) resistors attached to the battery surface. A Speedgoat Baseline real-time target machine is implemented to generate the PWM drive signals and log the measured battery temperatures during self-heating.

Before the tests all battery cells are charged to 4.0V (SOC=0.8) and soaked at -20 ˚C in a thermal chamber for 6 hours. Considering the size and efficiency of the RBSH, f_r is chosen as 40 kHz. The RBSH with different designed parameters heats the battery cells from -20 ˚C to 0 ˚C, as shown in Fig. 10.

A resonant tank of L_r=9.5 μH and C_r=1.66 μF (Z_r=2.4 Ω) is first used to evaluate the influence of f_s on the RBSH. In the tests, f_s is set to 19.8 kHz, 18.0 kHz, and 16.8 kHz, respectively. The corresponding experimental waveforms are depicted in Fig. 11. It is clear that the heating current amplitude and cut-off current both increase with the reduced f_s, which verifies to the analytical model. The influence of f_s on battery heating speed is shown in Fig. 12, where the warm-up periods from -20 ˚C to 0 ˚C are 660s, 550s, and 397s, respectively. The lower f_s can improve the warm-up speed due to the higher induced heating current, as described in (6). However, according to (7), the lower f_s results in high cut-off current, causing surging voltage spikes during turn-off, as shown in Fig. 11 (c). Thus, the efficiency and reliability of the RBSH are degraded if Z_r is not optimized for keeping f_s closed to f_r/2.

Based on the proposed non-linear optimization programming from (15), the optimized RBSH parameters are listed in Table I together with the design constraints. It can be seen that the optimized f_s is nearly $0.42f_r$, which drifts away from f_r/2. The reason is that the battery impedance R_b cannot be neglected compared to Z_r=1.5 Ω. According to (4), the actual resonant frequency is reduced to 38.6 kHz, for which f_s should be further decreased to obtain enough ZVS capability. To validate the proposed optimized design, the experimental tests with Z_r=2.4 Ω (L_r=9.5 μH, C_r=1.66 μH) and Z_r=3.0 Ω (L_r=12.0 μH, C_r=1.33 μH) are also conducted for performance comparison, in addition to the design values from Table I. According to (9), f_s is respectively tuned to 15.6 kHz and 15.0 kHz for Z_r=2.4 Ω and Z_r=3.0 Ω in order to generate the same peak discharge currents (9A) of the RBSH. Thus, almost identical warm-up periods can be ensured for the RBSH.

The corresponding experimental waveforms are shown in Fig. 13 and 14. As depicted in Fig. 13(a), the cut-off current i_{off} is 0.22A at T_{bat}=-20ºC with the proposed optimized design, guaranteeing the ZVS capability without sacrificing the efficiency. With higher Z_r, f_s is tuned down to achieve comparable heating speed. Nevertheless, the tuned switching frequency raises higher turn-off currents (4.1 A and 3.8 A) inevitably, producing the undesirable voltage spikes and surging turn-off losses, as shown in Fig. 13(b) and (c).

The temperature-dependent performance of the RBSH is also presented. From Fig. 13(a) and Fig. 14(a), it is clear that the peak charge/discharge currents and cut-off current are almost kept identical at T_{bat}=0ºC and T_{bat}=-20ºC with the proposed

This article has been accepted for publication in a future issue of this journal, but has not been fully edited. Content may change prior to final publication. Citation information: DOI 10.1109/TTE.2020.3025014, IEEE Transactions on Transportation Electrification

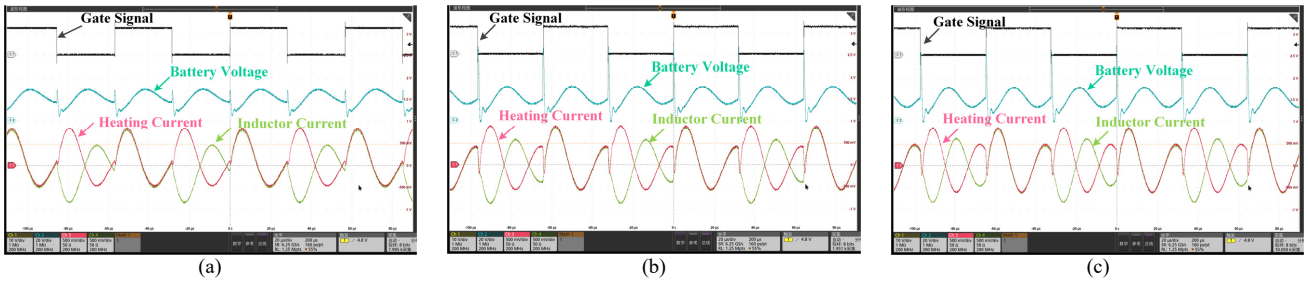

Fig. 13. Experimental waveforms of the RBSH at T_{bat}=-20 ºC: (a) Z_r=1.5Ω, f_s=16.8 kHz; (b) Z_r=2.4Ω, f_s=15.6 kHz, (c) Z_r=3.0Ω, f_s=15.0 kHz.

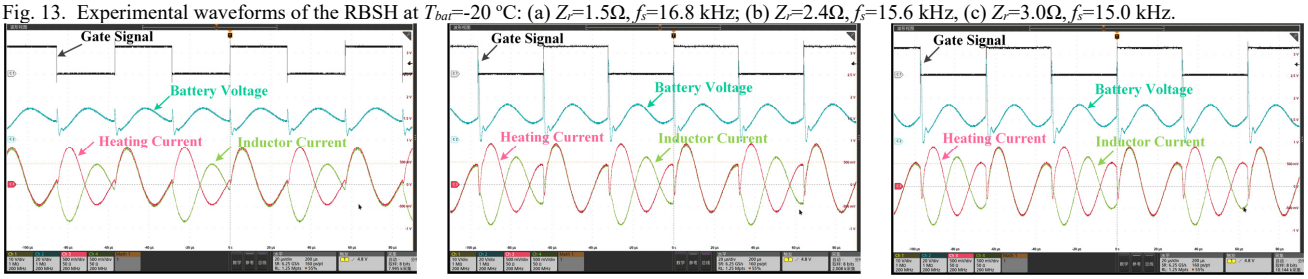

Fig. 14. Experimental waveforms of the RBSH at T_{bat}=0 ºC: (a) Z_r=1.5Ω, f_s=16.8 kHz; (b) Z_r=2.4Ω, f_s=15.6 kHz, (c) Z_r=3.0Ω, f_s=15.0 kHz.

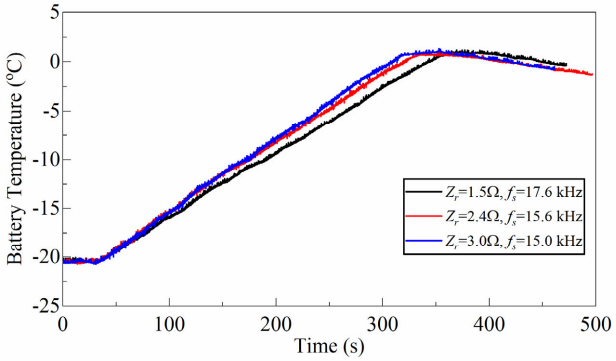

Fig. 15. Battery temperature during self-heating with I_{ch_max}=9.0A (3C) at different Z_r and f_s.

optimized design, so that the excessive switching losses and battery capacity fade can be avoided during the entire warm-up period. On the contrary, with Z_r=2.4 Ω and 3.0 Ω, the rising temperature leads to increasing peak heating currents (9.5 A and 9.6 A) of the RBSH, which exceeds the charge/discharge limitations at T_{bat}=0 ˚C. Meanwhile, the rising temperature also affects the cut-off currents of the RBSH, whose values are 4.4 A and 4.0 A at T_{bat}=0 ˚C. The experimental results correspond to the theoretical analysis shown in Fig. 7 that the peak charge/discharge currents and cut-off currents are strongly dependent on the battery temperature if the RBSH parameters are not properly optimized.

The cell temperatures during self-heating with different Z_r are shown in Fig. 15. Initially, the temperature rising rates at are almost identical because the designed heating currents at -20° C are the same. The temperature rising rate with a higher Z_r gradually exceeds that of the optimized design with the rising cell temperature due to the decreased R_b. Therefore, the whole warm-up periods for Z_r=1.5 Ω (optimized), 2.4 Ω, and 3.0 Ω are 314s, 289s, and 276s, respectively.

To validate the energy-efficient performance of the proposed optimized design, the switching and conduction losses of power switches are measured together with the resonant tank losses. As ZVS is guaranteed, the switching losses are calculated by integrating the product of V_{DS} and i_{bat} during only turn-off intervals, as shown in Fig. 16. The conduction losses and passive component losses can be achieved in the similar approach. The loss analysis results of the RBSH with different Z_r and f_s are shown in Fig. 17. The calculated switching losses P_{sw} are 0.213 W, 0.864 W, and 0.899 W with Z_r=1.5 Ω, 2.4 Ω, and 3.0 Ω, respectively. The conduction losses P_{cond} and resonant tank losses P_{tank} are all around 1.75 W and 0.72 W, respectively. It is clear that the higher battery heating rates with higher Z_r are obtained at the price of switching losses. The optimized RBSH parameters can effectively reduce the switching losses, while other types of losses are almost identical compared to those with other Z_r and f_s.

The cells are warmed up for 4 times in a row with different Z_r and f_s. The energy consumptions are calculated from the pre-calibrated SOC-OCV curve shown in Fig. 18, which indicates that 5.02%, 5.74%, and 6.61% of the cell energy are consumed for warming up the cell from -20° C to 0° C with Z_r=1.5 Ω (optimized), 2.4 Ω, and 3.0 Ω, respectively. Hence, the experimental results demonstrate that the optimized design of the resonant self-heater is effective in improving the system efficiency as well as the reliability by eliminating the surging cut-off currents.

To illustrate the merits of the RBSH with the optimized design, a systematic comparison is conducted with four other self-heating configurations. Detailed comparison results are shown in Table II, where the heating speed, energy consumption, and heater size are included.

For the pulse-heating scheme in [13], extra ultracapacitors are employed to generate low-frequency (10 Hz) pulse heating current, resulting in a large size and cost for onboard applications. In [25], the heating efficiency of the Buck-Boost-type self-heater is degraded due to hard-switching operations, which also limits the compactness of the heater. For the RBSH in [26] and [28], the switching frequency and characteristic impedance of the resonant tank are not optimized from the systematic perspective, whose cut-off current is not sufficient

This article has been accepted for publication in a future issue of this journal, but has not been fully edited. Content may change prior to final publication. Citation information: DOI 10.1109/TTE.2020.3025014, IEEE Transactions on Transportation Electrification

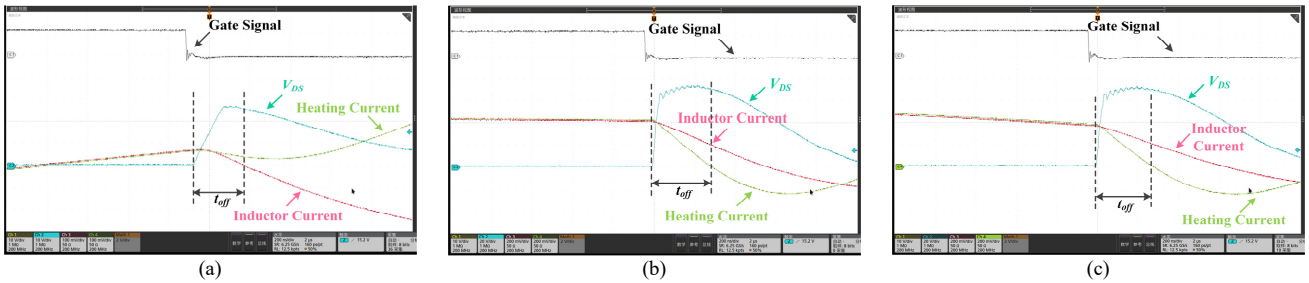

(a) (b) (c)

Fig. 16. Experimental waveforms of the RBSH at turn-off intervals: (a) Z_r=1.5Ω, f_s=16.8 kHz; (b) Z_r=2.4Ω, f_s=15.6 kHz, (c) Z_r=3.0Ω, f_s=15.0 kHz.

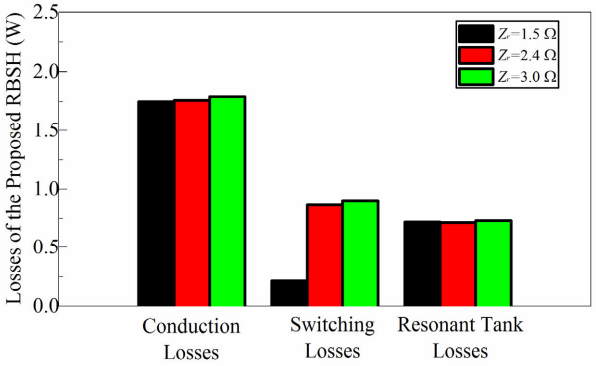

Fig. 17. Loss breakdowns of the RBSH with different Z_r.

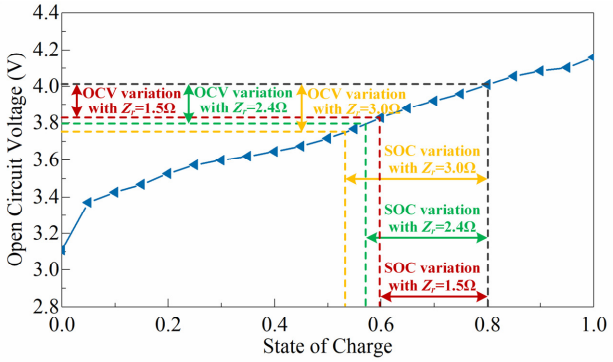

Fig. 18. OCV and SOC variations of the cells after 4 times self-heating in a row with different RBSH parameters.

TABLE II.
A COMPARISON OF INTERNAL AC HEATING SCHEMES

Heating Method	Ambient Temperature	RMS Current	Heating Frequency	Heating Speed	Energy Consumption	Heater Size
Low-frequency Pulse Heating [13]	-20°C	3.1C	10 Hz	7.10°C/min	0.295%/°C	Large
Buck-Boost Heater [25]	-20°C	2.87C	7 kHz	3.42°C/min	0.530%/°C	Medium
Non-optimized RBSH I [26]	-20°C	2.72C	754 Hz	2.29°C/min	0.332%/°C	Medium
Non-optimized RBSH II [28]	-20°C	1.54C	80 kHz	2.63°C/min	0.280%/°C	Small
Proposed optimized RBSH	-20°C	2.12C	36.5 kHz	3.82°C/min	0.251%/° C	Small

to realize ZVS capability. Thus, the energy-efficiency is not minimized for heating Li-ion cells from -20° C to 0° C. For the proposed optimized RBSH, the parameters are designed by considering overall performance, including heating speed, efficiency, and ZVS capability, etc. Hence, the consumed energy for self-heating Li-ion cells is minimized with the proposed optimized RBSH, which is particularly suitable for EV batteries.

VI. CONCLUSION

Onboard resonant battery self-heater is a promising solution for EVs to alleviate Li-ion batteries' performance degradation at cold climates. Due to the parametric sensitivity of the resonant converter, the heating performance of the RBSH highly relies on the initial parameter design, while no theoretical design methodology is developed to deal with the complex constraints. Hence, an analytical model of the RBSH is first proposed to illustrate the influence of the designed parameters on heating speed, efficiency, and reliability. Based on the developed RBSH model, it is concluded that the switching frequency f_s and characteristic impedance Z_r are the most significant parameters related to the heating performance, and the RBSH design can be formulated as a nonlinear optimization problem for searching the minimum Z_r within the constraints of the maximum charge/discharge current and cut-off current. The Adaptive Genetic Algorithm is applied in this study to solve the optimum f_s and Z_r, so that the heating speed, efficiency, and reliability of the RBSH can be comprehensively optimized.

Several downscaled experiments are conducted to validate the effectiveness of the proposed design methodology. The RBSH under an optimal design warms up the Li-ion cells rapidly from -20°C to 0°C within 314 s and only consumes 5.01% of the cell energy, showing superior performance beyond other groups of RBSHs. It is evident that the proposed design methodology contributes to alleviating the EV range anxiety and charging dilemma in winter.

REFERENCE

[1] A. Emadi, Y. Lee, and K. Rajashekara, "Power electronics and motor drives in electric, hybrid electric, and plug-in hybrid electric vehicles," *IEEE Trans. Ind. Electron.*, vol. 55, no. 6, pp. 2237-2245, May 2008.

[2] S. Williamson, A. Rathore, and F. Musavi, "Industrial electronics for electric transportation: current state-of-the-art and future challenges," *IEEE Trans. Ind. Electron.*, vol. 62, no. 5, pp. 3021-3032, May 2015.

[3] J. Jaguemont, L. Boulon, P. Venet, Y. Dube, and A. Sari, "Lithium-ion battery aging experiments at subzero temperatures and model development for capacity fade estimation," *IEEE Trans. Veh. Technol.*, vol. 65, no. 6, oo. 4328-4343, Jun. 2016.

[4] J. Jaguemont, L. Boulon, Y. Dube, and F. Martel, "Thermal management

of a hybrid electric vehicle in cold weather," *IEEE Trans. Energy Convers.*, vol. 31, no. 3, pp. 1110–1120, Sept. 2016.

[5] J. Jaguemont, L. Boulon, and Y. Dube, "Characterization and modeling of a hybrid-electric-vehicle lithium-ion battery pack at low temperatures," *IEEE Trans. Veh. Technol.*, vol. 65, no. 1, pp. 1–14, Jan. 2016.

[6] M. Ouyang, Z. Chu, L. Lu, J. Li, X. Han, X. Feng, and G. Liu, "Low temperature aging mechanism identification and lithium deposition in a large format lithium iron phosphate battery for different charge profiles," *J. Power Sources*, vol. 286, pp. 309-320, Jul. 2015.

[7] K. Liu, Y. Li, X. Hu, M. Lu, and W. Windanage, "Gaussian process regression with automatic relevance determination kernel for calendar aging prediction of lithium-ion batteries," *IEEE Trans. Ind. Informat.*, vol. 16, no. 6, pp. 3767-3777, Jun. 2020.

[8] K. Liu, X. Hu, Z. Wei, Y. Li, and Y. Jiang, "Modified gaussian process regression models for cyclic capacity prediction of lithium-ion batteries," *IEEE Trans. Transport. Electrific.*, vol. 5, no. 4, pp. 1225-1235, Dec. 2019.

[9] X. Yang, G. Zhang, S. Ge, and C. Wang, "Fast charging of lithium-ion batteries at all temperatures," *Proc. Natl. Acad. Sci. U.S.A.*, vol. 115, no. 28, pp. 7266-7271, Jul. 2018.

[10] K. Liu, X. Hu, Z. Yan, Y. Xie, and S. Feng, "Lithium-ion battery charging management considering economic costs of electrical energy loss and battery degradation," *Energy Convers. Manage.*, vol. 195, pp. 167-179, 2019.

[11] X. Hu, Y. Zheng, D. Howey, H. Perez, A. Foley, and M. Pecht, "Battery warm-up methodologies at subzero temperatures for automotive applications: recent advances and perspectives," *Prog. Energy Combust. Sci.*, vol. 77, pp. 1-28, Mar. 2020.

[12] C. Vidal, O. Gross, R. Gu, P. Kollmeyer, and A. Emadi, "xEV Li-ion battery low-temperature effects—review," *IEEE Trans. Veh. Technol.*, vol. 68, no. 5, May 2019.

[13] S. Mohan, Y. Kim, and A. Stefanopoulou, "Energy-conscious warm-up of Li-ion cells from subzero temperatures," *IEEE Trans. Ind. Electron.*, vol. 63, no. 5, pp. 2954-2964, May 2016.

[14] J. Zhang, H. Ge, Z. Li, and Z. Ding, "Internal heating of lithium-ion batteries using alternating current based on the heat generation model in frequency domain," *J. Power Sources*, vol. 273, pp. 1030-1037, Jan. 2015.

[15] H. Ruan, J. Jiang, B. Sun, W. Zhang, W. Gao, L. Wang, and Z. Ma., "A rapid low-temperature internal heating strategy with optimal frequency based on constant polarization voltage for lithium-ion batteries," *Appl. Energy*, vol. 177, pp. 771–782, Sep. 2016.

[16] J. Zhu, Z. Sun, X. Wei, H. Dai, and W. Gu, "Experimental investigation of an AC pulse heating method for vehicular high power lithium-ion batteries at subzero temperatures", *J. Power Sources*, vol. 367, pp. 145-157, Nov. 2017.

[17] J. Li, D. Sun, Z. Chai, H. Jiang, and C. Sun, "Sinusoidal alternating current heating strategy and optimization of lithium-ion batteries with a thermo-electric coupled model", *Energy*, vol. 186, pp. 1-13, 2019.

[18] H. Ge, J. Huang, J. Zhang, and Z. Li, "Temperature-adaptive alternating current preheating of lithium-ion batteries with lithium deposition prevention," *J. Electrochem. Soc.*, vol. 163, no. 2, pp. A290-A299, 2015.

[19] S. Guo, R. Xiong, K. Wang, and F. Sun, "A novel echelon internal heating strategy of cold batteries for all-climate electric vehicles applications", *Appl. Energy*, vol. 219, pp. 256-263, Jun. 2018.

[20] Q. Wang, Y. He, J. Shen, X. Hu, and Z. Ma, "State of charge-dependent polynomial equivalent circuit modeling for electrochemical impedance spectroscopy of lithium-ion batteries," *IEEE Trans. Power Electron.*, vol. 33, no. 10, pp. 8449-8460, Oct. 2018.

[21] Y. Shang, N. Cui, B. Duan, and C. Zhang, "Analysis and optimization of star-structured switched-capacitor equalizers for series-connected battery strings," *IEEE Trans. Power Electron.*, vol. 33, no. 11, pp. 9631-9646, Nov. 2018.

[22] Y. Shang, C. Zhang, N. Cui, and J. Guerrero, "A cell-to-cell battery equalizer with zero-current switching and zero-voltage gap based on quasi-resonant LC converter and boost converter," *IEEE Trans. Power Electron.*, vol. 30, no. 7, pp.3731-3747, Jul. 2015.

[23] Y. Shang, B. Xia, N. Cui, C. Zhang, and C. Mi, "An automotive onboard AC heater without external power supplies for Lithium-Ion batteries at low temperatures," *IEEE Trans. Power Electron.*, vol. 33, no. 9, pp. 7759-7769, Sep. 2018.

[24] Y. Shang, C. Zhu, Y. Fu, C. Mi, "An integrated heater equalizer for lithium-ion batteries of electric vehicles", *IEEE Trans. Ind. Electron.*, vol. 66, no. 6, pp. 4398-4405, Jun. 2016.

[25] C. Zhu, Y. Shang, F. Lu, Y. Jiang, C. Cheng, and C. Mi, "Core temperature estimation for self-heating automotive lithium-ion batteries in cold climates," *IEEE Trans. Ind. Informat.*, vol. 16, no. 5, pp. 3366-3375, May 2020.

[26] J. Jiang, H. Ruan, B. Sun, L. Wang, W. Gao, and W. Zhang, "A low-temperature internal heating strategy without lifetime reduction for large-size automotive lithium-ion battery pack", *Appl. Energy*, vol. 230, pp. 257-266, 2018.

[27] Y. Shang, K. Liu, N. Cui, N. Wang, K. Li, and C. Zhang, "A compact resonant switched-capacitor heater for lithium-ion battery self-heating at low temperatures," *IEEE Trans. Power Electron.*, vol. 35, no. 7, pp. 7134-7144, Jul. 2020.

[28] Y. Shang, K. Liu, N. Cui, Q. Zhang, and C. Zhang, "A sine-wave heating circuit for automotive battery self-heating at subzero temperatures," *IEEE Trans. Ind., Informat.*, vol. 16, no. 5, pp. 3355-3365, May 2020.

[29] C. Zhu, Y. Shang, F. Lu, and H. Zhang, "Optimized design of an onboard resonant self-heater for automotive lithium-ion batteries at cold climates," in *Proc. IEEE Energy Convers. Congr. Expo.*, 2019, pp. 5084-5088.

[30] K. Liu, C. Zou, K. Li, and T. Wik, "Charging pattern optimization for lithium-ion batteries with an electrothermal-aging model," *IEEE Trans. Ind., Informat.*, vol. 14, no. 12, pp. 5463-5474, Dec. 2018.

[31] L. Zheng, J. Zhu, G. Wang, D. Lu, T. He, "Lithium-ion battery instantaneous available power prediction using surface lithium concentration of solid particles in a simplified electrochemical model," *IEEE Trans. Power Electron.*, vol. 33, no. 11, pp. 9551-9560, Nov. 2018.

[32] S. Li, W. Li, J. Deng, T. Nguyen, and C. Mi, "A double-sided LCC compensated network and its tuning method for wireless power transfer," *IEEE Trans. Veh. Technol.*, vol. 64, no. 6, pp. 2261-2273, Jun. 2015.

[33] M. Srinivas, and L. Patnaik, "Adaptive probabilities of crossover and mutation in genetic algorithms," *IEEE Trans. Syst. Man. Cy.*, vol. 24, no. 4, pp. 656-667, Apr. 1994.

Chong Zhu (M'17) received the B.S. degree in electrical engineering from China University of Mining and Technology, Xuzhou, China, in 2010 and the Ph. D. degree in electrical engineering from Zhejiang University, Hangzhou, China, in 2016. He was a Postdoctoral Researcher with San Diego State University, San Diego, CA, USA from 2017 to 2019.

He is currently an Assistant Professor with the School of Mechanical Engineering in Shanghai Jiao Tong University, Shanghai, China. His research interests include battery thermal management, design and control of power converters applied in electric vehicles.

Yue Cao (Member, IEEE) received the B.S. degree (Hons.) in electrical engineering with a second major in mathematics from the University of Tennessee, Knoxville, TN, USA, in 2011, and the M.S. and Ph.D. degrees in electrical engineering from the University of Illinois at Urbana–Champaign (UIUC), Champaign, IL, USA, in 2013 and 2017, respectively.

Dr. Cao is currently an Assistant Professor with the Energy Systems Group at Oregon State University (OSU), Corvallis, OR, USA. Before joining OSU, he was a Research Scientist with the Propulsions Team at Amazon Prime Air in Seattle, WA, USA. He was a Power Electronics Engineer Intern with Special Projects Group at Apple Inc., Cupertino, CA, USA; Halliburton Company, Houston, TX, USA; Flanders Electric, Evansville, IN, USA; and Oak Ridge National Laboratory, Oak Ridge, TN, USA. He was a Sundaram Seshu Fellow in 2016 at UIUC, where he was a James M. Henderson Fellow in 2012. His research interests include power electronics, motor drives, and energy storage with applications in transportation electrification, renewable energy integration, and energy-efficient buildings.

Dr. Cao received the Myron Zucker Award from the IEEE Industry Applications Society (IAS) in 2010. He was a recipient of Oregon State Learning Innovation Award for transformative education in 2020. He was the

Corresponding Technical Programs Chair of the 2016 IEEE Power and Energy Conference at Illinois (PECI). He was the Local and Industry Co-Chair of the 2018 IEEE Energy Conversion Congress Expo (ECCE). He was the Panel Chair on More Electric Aircraft at the 2019 IEEE International Transportation Electrification Conference (ITEC). He is currently the Tutorials Chair of ECCE 2021. In 2020, he helped establish a joint IEEE PES/PELS Chapter at OSU. He is currently an Associate Editor for IEEE Transactions on Transportation Electrification.

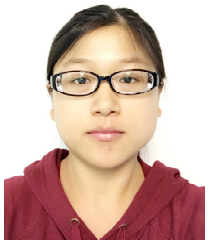

Hua Zhang (S'14–M'17) received B.S., M.S. and PhD degree in electrical engineering from Northwestern Polytechnical University, Xi'an, China, in 2011, 2014, and 2017, respectively.

From September 2014 to August 2015, she was a joint Ph.D. student founded by the China Scholarship Council with the University of Michigan, Dearborn. From September 2015, she started to work in San Diego State University. She is now a postdoctoral research associate in Drexel University, PA, USA. Her research is about the charging technology of electric vehicles.

Fei Lu (S'12–M'17) received the B.S. and M.S. degree from Harbin Institute of Technology, Harbin, China, in 2010 and 2012, respectively, and the PhD degree from University of Michigan, Ann Arbor, Michigan, USA, in 2017, all in electrical engineering.

He is currently an assistant professor in the Department of Electrical and Computer Engineering in Drexel University, Philadelphia, PA, USA. His research topic focuses on power electronics and the application of electric vehicle charging.

Xi Zhang received the B.Sc. degree in Applied Mathematics and the B.E. degree in Information and Control Engineering from Shanghai Jiao Tong University (SJTU), Shanghai, China in 2002. He received the M.E. and Ph.D. degrees in Power Electronics and Electric Power Drive from SJTU, in 2004 and 2007, respectively. From September 2007 to July 2009, he held a postdoctoral position with the Department of Electrical and Computer Engineering, the University of Michigan-Dearborn, Dearborn, MI, USA. He is currently the professor with the Institute of Automotive Engineering and National Engineering Lab for Automotive Electronics and Control Technology, SJTU. His research interests include wireless charging, power management strategies, power electronics devices and motor control systems of EV/HEV.